



Cite this: *RSC Adv.*, 2021, 11, 30943

# A bio-based phosphaphenanthrene-containing derivative modified epoxy thermosets with good flame retardancy, high mechanical properties and transparency

Wei Peng, Yu-xuan Xu, Shi-bin Nie \* and Wei Yang

Phosphorus-containing flame retardants have received huge interest for improving the flame retardant behavior of epoxy resins (EP) over the past few decades. However, a satisfactory flame retardant effect requires high loading of most phosphorus-containing flame retardants, resulting in the deterioration of the thermo-mechanical properties of the flame retardant epoxy materials. To obtain the flame retardant EP with excellent comprehensive properties, a furfurylamine-derived bis-DOPO derivative (FA-bis-DOPO) was synthesized from bio-mass as a co-curing agent for the flame retardant EP. The incorporation of FA-bis-DOPO improved the mechanical strength, the storage modulus and the glass transition temperature of the flame retardant epoxy materials, owing to its stiffness and reactivity with the epoxy matrix to enhance the crosslinking density. The EP material containing 5.0 wt% of FA-bis-DOPO had an LOI of 31.0% and UL-94 V-0 rating, while the pristine EP had an LOI of 23.5% and failed in the UL-94 test, manifesting the high flame retardant efficiency of FA-bis-DOPO. Besides, the cone calorimeter results demonstrated that the PHRR, THR, and TSP values of the EP/FA-bis-DOPO-5.0 were 28.0%, 27.3%, and 9.9% lower than those of the pristine EP, respectively. The flame retardant mechanism of FA-bis-DOPO could be attributed to the combined vapor and condensed phase mechanisms which involved the interruption of the combustion chain reaction by quenching radicals and the inhibition of the transfer of pyrolytic volatile products by catalytic formation of an intact and compact char layer.

Received 26th July 2021  
Accepted 5th September 2021

DOI: 10.1039/d1ra05709j

rsc.li/rsc-advances

## 1. Introduction

Among various thermosetting materials, epoxy resin has many excellent properties, such as excellent thermal stability, outstanding bonding performance, dimensional stability and corrosion resistance, high mechanical strength and low dielectric properties.<sup>1–8</sup> Therefore, epoxy resin is widely used in coating, construction, medicine, electronics, aerospace and other fields. However, the flammability of epoxy resin blocks the development and application of epoxy resin. Pure epoxy resin burns rapidly after ignition, and produces a large amount of smoke, which has a great fire risk. The epoxy resin needs to be flame retardant in many applications.

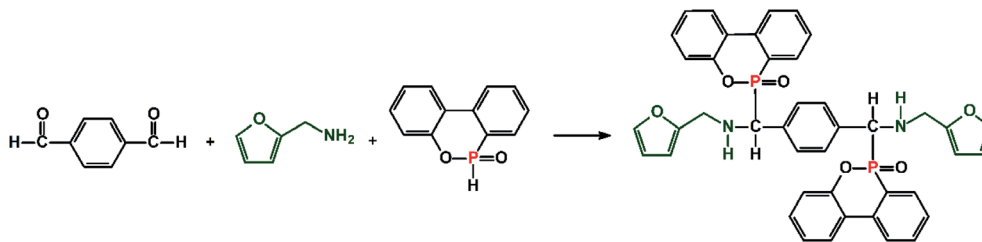
Halogenated flame retardants are a major member of commercial flame retardants, because halogenated flame retardant has very high flame retardant efficiency, which can greatly increase the flame resistance of materials, so that the materials meet the flame retardant requirements. However, the halogenated flame retardant will release a large number of toxic hydrogen halide gases during the combustion, which will damage the respiratory system of human beings and have certain destructive

effect on the environment.<sup>9,10</sup> With the increasing concerns on the green development, halogen-free flame retardants are imperative. Phosphorus-containing flame retardant is an important halogen-free flame retardant. Because of its good flame retardant effect and green environment protection characteristics, phosphorus-containing flame retardant is favored by many researchers from both academic and industrial fields.<sup>11,12</sup>

DOPO, as an attractive phosphorus-containing flame retardant, has attracted extensive attention in recent years.<sup>13</sup> Because of the highly active P–H bond in its molecule, DOPO can react with epoxy group, C=C bond, carbonyl group, Schiff base, and amino group to prepare a series of DOPO derivatives.<sup>14</sup> Compared with traditional halogen-containing flame retardants, DOPO derivatives not only have good flame retardant effect, but also are not easy to produce toxic gases. Therefore, DOPO derivatives are considered as one of the most likely alternatives to halogenated flame retardants in the future. Yang *et al.*<sup>15</sup> synthesized a phosphorus- and nitrogen-containing flame retardant based on triazine (DOPO-TMT), and used it as additive to prepare the cured flame retardant epoxy thermoset. The limiting oxygen index (LOI) of the flame retardant epoxy thermoset was up to 36.2% at 1 wt% phosphorus content, and it could pass UL-94 V-0 grade. Xu *et al.*<sup>16</sup> synthesized a flame

School of Safety Science and Engineering, Anhui University of Science and Technology, Huainan 232001, P. R. China. E-mail: nieshibin88@163.com





Scheme 1 The synthetic route of FA-bis-DOPO.

retardant based on cyclotriphosphazene and DOPO, and incorporated it to the cured flame retardant epoxy thermoset, showing good flame retardant effect. When the phosphorus content in the resin reached 1.1 wt%, the flame retardant epoxy resin can pass UL-94 V-0 test, and the LOI reached 36.6%. Qian *et al.*<sup>17</sup> reported a halogen-free flame retardant based on DOPO and triazine (TGIC-DOPO) for the preparation of epoxy resin with excellent flame retardant effect. When the content of flame retardant reaches 12%, the flame retardant epoxy resin can pass UL-94 V-0 test, and the LOI reached 33.3%. Wang *et al.*<sup>3</sup> synthesized an oligomer containing DOPO. After curing, the flame retardant epoxy resin had excellent flame retardant performance and significantly increased glass transition temperature. At 15% addition, it can pass UL-94 V-0 grade, and the LOI was as high as 36%. Although these DOPO-based derivatives have good flame retardant effect on epoxy resin, there are still some problems, such as high addition amount, poor mechanical properties and poor compatibility with the matrix. Therefore, the development of more efficient DOPO-derived flame retardants remains a challenging work.

In recent years, development of flame retardants from bio-based masses has been one of research hot spots. Among various bio-based masses, furan-based compounds stand out for their unique five membered oxygen-containing heterocyclic structure, and are regarded as one of the ten most valuable bio based compounds by the U.S. Department of Energy.<sup>18</sup> Furan-based compounds are environment-friendly green materials, which can be produced from agricultural wastes, such as rice husk, corncob and bagasse. In this study, a bio-based bis-DOPO derivative (FA-bis-DOPO) was synthesized by the addition reaction among DOPO, *p*-phthalaldehyde, and furfurylamine. Because of the presence of the secondary amine in the structure, FA-bis-DOPO was used as a co-curing agent for the fabrication of the flame retardant epoxy thermosets. The molecular structure of FA-bis-DOPO was checked by FTIR and NMR spectra. The effect of FA-bis-DOPO on the thermal stability, mechanical strength, and anti-flammable behaviors of the resulting EP thermosets were studied, and the flame retardant mechanism was clarified as well.

## 2. Experimental

### 2.1. Materials

Diglycidyl ether of bisphenol A (DGEBA) epoxy resin (epoxy value: 0.44 mol/100 g) was purchased from Shanghai Macklin Biochemical Co., Ltd, China. 9,10-Dihydro-9-oxa-10-phosphaphenanthrene-10-oxide (DOPO), *p*-phthalaldehyde, furfurylamine, and 4,4'-diaminodiphenylmethane (DDM) were supplied by Shanghai Aladdin Chemicals Company, China. Anhydrous ethanol was provided by Sinopharm Chemical Reagent Co., Ltd, China.

### 2.2. Synthesis of bio-based bis-DOPO derivative (FA-bis-DOPO)

Furfurylamine (19.42 g, 0.2 mol), *p*-phthalaldehyde (13.42 g, 0.1 mol), and anhydrous ethanol (200 mL) were introduced into a 500 mL 3-necked round bottom flask equipped with a condenser, a magnetic stirrer, and a nitrogen inlet. The mixture was stirred at 70 °C for 8 h under nitrogen atmosphere. Then, DOPO (43.24 g, 0.2 mol) was charged to the reaction system and stirred for another 24 h. The solvent was removed by a rotary evaporator, and then the precipitate was washed with cooled ethanol three times. The obtained product was dried in a vacuum oven at 80 °C overnight. The synthetic route of FA-bis-DOPO is illustrated in Scheme 1.

### 2.3. Preparation of the cured epoxy thermosets

The FA-bis-DOPO powder was added to DGEBA epoxy resin at 100 °C under stirring for 30 min to obtain a uniform mixture. Then, DDM was introduced to the above mixture at an equivalent molar ratio of N-H and epoxy groups. The mixture was stirred for another 10 min and then poured into the mold immediately. The curing process was 100 °C for 2 h, 150 °C for 2 h, and 180 °C for 1 h. The formulations of the cured epoxy thermosets containing 0, 2.5, and 5.0 wt% FA-bis-DOPO are listed in Table 1. The pristine epoxy thermoset was prepared using the same procedure just without adding FA-bis-DOPO.

Table 1 The formulations of the cured epoxy thermosets

Sample	DGEBA (g)	DDM (g)	FA-bis-DOPO (g)	Theoretical P content (wt%)
EP	82.1	17.9	0	0
EP/FA-bis-DOPO-2.5	80.3	17.2	2.5	0.21
EP/FA-bis-DOPO-5.0	78.6	16.4	5.0	0.43



## 2.4. Characterization

A Shimadzu IRAffinity-1 Fourier transform infrared (FTIR) spectrometer was employed to record the FTIR spectra of the samples using a KBr disc method. The proton and phosphorus nuclear magnetic resonance (NMR) spectra of the samples were collected by a Bruker AVANCE NMR spectrometer (400 MHz) using deuterated chloroform as solvent. Elemental analysis was conducted on an Elementar Vario EL-III analyzer. The curing process was monitored by the TA Q2000 differential scanning calorimetry (DSC). The samples were heated at a ramp rate of  $10.00\text{ }^{\circ}\text{C min}^{-1}$  to  $250.0\text{ }^{\circ}\text{C}$ . Tensile property of the samples was measured by an Instron-5967 universal electronic testing machine following the ASTM D638 specification at a crosshead rate of  $2.0\text{ mm min}^{-1}$ . The reported data were averaged from at least five parallels. Dynamic mechanical analysis (DMA) was performed on a TA Q850 analyzer. The ramp rate was  $5\text{ }^{\circ}\text{C min}^{-1}$  from  $30$  to  $200\text{ }^{\circ}\text{C}$ . Thermogravimetric analysis (TGA) was measured by a Mettler-Toledo TGA/SDTA851e thermo-analyzer under both nitrogen and air conditions. The ramp rate was  $20\text{ }^{\circ}\text{C min}^{-1}$  from  $30$  to  $700\text{ }^{\circ}\text{C}$ . The limiting oxygen index (LOI) of the samples (Size:  $127\text{ mm} \times 6.5\text{ mm} \times 3.2\text{ mm}$ ) was determined by a TTech-GBT406 oxygen index meter following the ASTM D2863-2017a specification. The UL-94 vertical burning performance of the samples (Size:  $127\text{ mm} \times 12.7\text{ mm} \times 3.2\text{ mm}$ ) was carried out by a CFZ-2-type apparatus following the ASTM D3801-2010 specification. An FTT cone calorimeter was employed to assess the flammability of the samples (Size:  $100\text{ mm} \times 100\text{ mm} \times 3\text{ mm}$ ) under  $50\text{ kW m}^{-2}$  following the ISO 5660-1 specification. The distance between the sample holder and the cone heater was set as  $25\text{ cm}$ . The reported data were averaged from triple parallels. TGA-FTIR technique was utilized to identify the pyrolytic volatile products during the thermal decomposition of the samples. The sample was heated in a TA Q50 TGA at a ramp rate of  $20\text{ }^{\circ}\text{C min}^{-1}$  from  $25$  to  $800\text{ }^{\circ}\text{C}$  under nitrogen condition. The pyrolytic volatile products were sent to the gas cell of a Nicolet 6700 FTIR spectrometer in real time through a stainless steel heating tube. To avoid the condensation of the pyrolytic volatile products, the stainless steel heating tube and the gas cell of the FTIR spectrometer were kept at  $230$  and  $250\text{ }^{\circ}\text{C}$ , respectively. A Gemini SEM 500 scanning electron microscopy (SEM) was employed to characterize the morphology of the residual chars at an accelerating voltage of  $3\text{ kV}$ . The micro-structure of the residual chars was measured by a Renishaw inVia Raman spectrometer using an excitation wavelength of  $532\text{ nm}$ .

## 3. Results and discussion

In order to confirm the successful synthesis of FA-bis-DOPO, FTIR was employed to check the molecular structure of FA-bis-DOPO. Fig. 1 gives the FTIR spectra of DOPO and FA-bis-DOPO. The FTIR spectrum of DOPO displays the characteristic peaks at  $3062\text{ cm}^{-1}$  (Ph-H),  $2434\text{ cm}^{-1}$  (P-H),  $1594\text{ cm}^{-1}$  (C=C in the aromatic ring),  $1236\text{ cm}^{-1}$  (P=O),  $1119$  and  $950\text{ cm}^{-1}$  (Ph-O-P).<sup>19</sup> In the FTIR spectrum of FA-bis-DOPO, the absence of the characteristic peak at  $2434\text{ cm}^{-1}$  corresponding

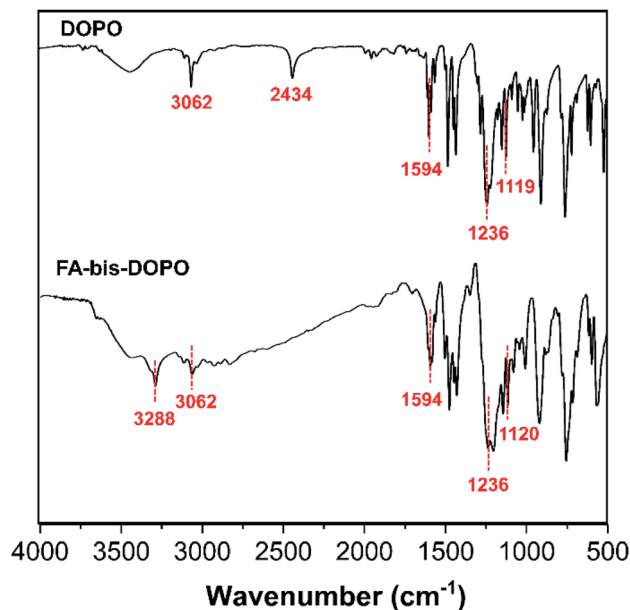


Fig. 1 FTIR spectra of DOPO and FA-bis-DOPO.

to the P-H bond of DOPO and the appearance of the characteristic peak at  $3288\text{ cm}^{-1}$  corresponding to the N-H bond of secondary amine imply the occurrence of the addition reaction among DOPO, furfurylamine, and *p*-phthalaldehyde.

NMR was further utilized to characterize the molecular structure of FA-bis-DOPO. Fig. 2 shows the proton and phosphorus NMR spectra of DOPO and FA-bis-DOPO. Comparing the proton NMR spectra of DOPO with that of FA-bis-DOPO, it can be found that the chemical shift at around  $8.90\text{ ppm}$  corresponding to the P-H bond of DOPO disappears in the proton

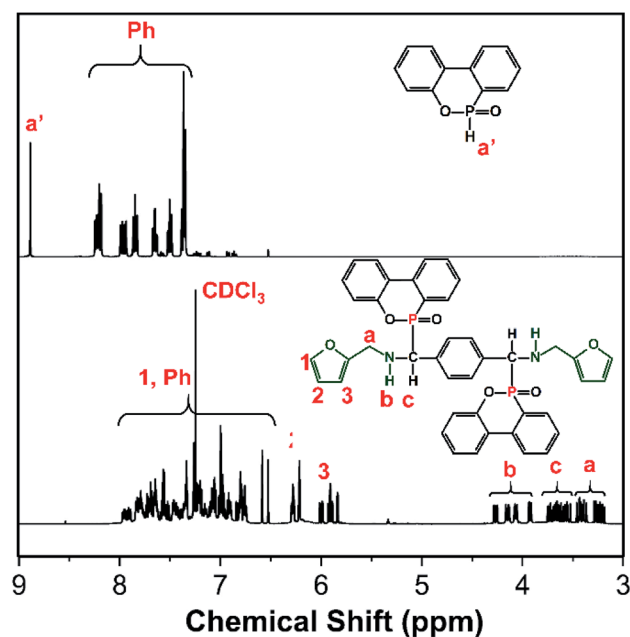


Fig. 2  $^1\text{H}$ -NMR spectra of DOPO and FA-bis-DOPO.

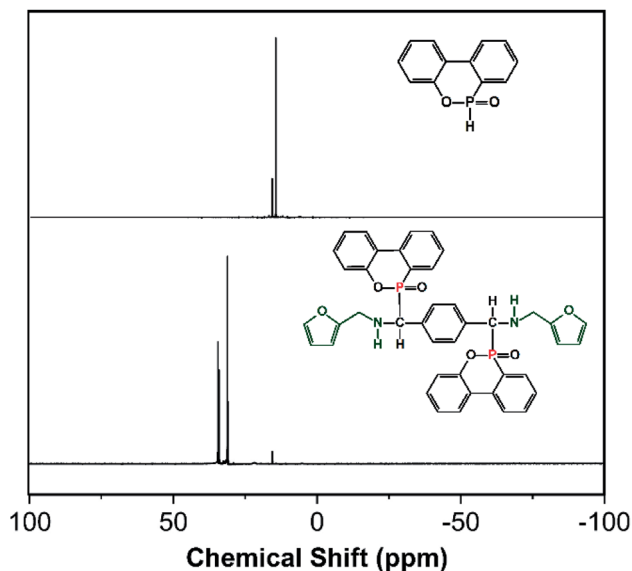


Fig. 3  $^{31}\text{P}$ -NMR spectra of DOPO and FA-bis-DOPO.

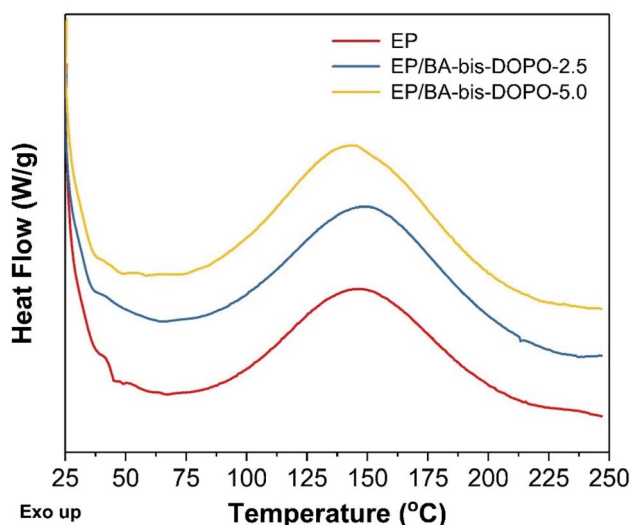


Fig. 4 The non-isothermal DSC thermograms of pure EP and EP/FA-bis-DOPO composites at a ramp rate of  $10\text{ }^{\circ}\text{C min}^{-1}$ .

NMR spectrum of FA-bis-DOPO, suggesting the completion of the addition reaction among DOPO, furfurylamine, and *p*-phthalaldehyde. Besides, all the other signals in the proton NMR spectrum of FA-bis-DOPO correspond well with the protons of the expected structure of FA-bis-DOPO, manifesting the successful synthesis of FA-bis-DOPO. Fig. 3 further displays

the phosphorus NMR spectra of DOPO and FA-bis-DOPO. The  $^{31}\text{P}$ -NMR spectrum of DOPO displays two signals at 14.5 and 15.9 ppm, indicating the existence of two chemical environments of the phosphorus atoms. For FA-bis-DOPO, there are also two signals at 30.9 and 33.1 ppm. This is because the chiral carbon and steric effect of DOPO unit results in the formation of two diastereomers of the target compound. This phenomenon has also been reported by the previous papers.<sup>16,20,21</sup> The elemental analysis of FA-bis-DOPO is measured to be 69.0% for carbon, 4.0% for nitrogen, and 13.5% for oxygen. These experimental values are very close to the theoretical values of 69.6% for carbon, 3.9% for nitrogen, and 13.3% for oxygen. Based on these results, it is confirmed that FA-bis-DOPO was successfully synthesized.

The performance of the cured thermosets has a strong dependence on their crosslinking state.<sup>22–29</sup> The non-isothermal DSC was utilized to investigate the curing characteristics of the pure EP and its composites. The DSC thermograms of pure EP and EP/FA-bis-DOPO composites are displayed in Fig. 4. It can be seen that all the samples exhibited a single exothermic peak during the curing process. The parameters of the exothermic peak include the onset temperature ( $T_{\text{onset}}$ ), peak temperature ( $T_{\text{p}}$ ), ending temperature ( $T_{\text{endset}}$ ), and enthalpy ( $\Delta H$ ), which are listed in Table 2.  $\Delta T$  is equal to  $T_{\text{endset}} - T_{\text{onset}}$ , and  $\Delta T^*$  and  $\Delta H^*$  are calculated by  $(\Delta T_{\text{EP/FA-bis-DOPO}}/\Delta T_{\text{neat EP}})$  and  $(\Delta H_{\text{EP/FA-bis-DOPO}}/\Delta H_{\text{neat EP}})$ , respectively. The curing index (CI) is computed by  $(\Delta T^* \times \Delta H^*)$ .<sup>30–33</sup> On the basis of the CI values, the curing state is classified into three ratings: Excellent ( $\Delta T^* < \text{CI} < \Delta H^*$ ), Good ( $\text{CI} > \Delta H^*$ ), and Poor ( $\text{CI} < \Delta T^*$ ).<sup>34,35</sup> As shown in Table 2, EP/FA-bis-DOPO-2.5 exhibited excellent curing state, and EP/FA-bis-DOPO-5.0 showed good curing state, because FA-bis-DOPO could participate in the curing reaction with the DGEBA pre-polymers. Owing to the excellent or good curing state, it is expected that FA-bis-DOPO will endow the cured thermosets with good flame retardancy, high mechanical property and transparency.<sup>34</sup>

FA-bis-DOPO was used as a co-curing agent for flame retardant epoxy thermosets. The photographs of the cured epoxy thermosets are given in Fig. 5. The pristine epoxy thermoset is light yellow color with high transparency. The color of the cured epoxy thermosets becomes yellow after FA-bis-DOPO is added. Furthermore, the color of the cured epoxy thermosets is deepened with increasing the FA-bis-DOPO amount. However, the EP/FA-bis-DOPO-5.0 is still highly transparent, indicating the molecular dispersion of FA-bis-DOPO within the epoxy networks.

The effect of FA-bis-DOPO on the mechanical property of the epoxy thermosets was studied by the tensile test. The typical stress-strain curves of the samples are given in Fig. 6. The

Table 2 Curing characteristics of the pure EP and its composites

Sample	$T_{\text{onset}} (^{\circ}\text{C})$	$T_{\text{p}} (^{\circ}\text{C})$	$T_{\text{endset}} (^{\circ}\text{C})$	$\Delta T (^{\circ}\text{C})$	$\Delta H (\text{J g}^{-1})$	$\Delta T^*$	$\Delta H^*$	CI	Rating
EP	93.6	148.2	236.7	143.1	141.3	—	—	—	—
EP/FA-bis-DOPO-2.5	92.4	151.6	227.2	134.8	159.3	0.94	1.13	1.06	Excellent
EP/FA-bis-DOPO-5.0	89.6	145.1	234.4	144.8	165.5	1.01	1.17	1.18	Good





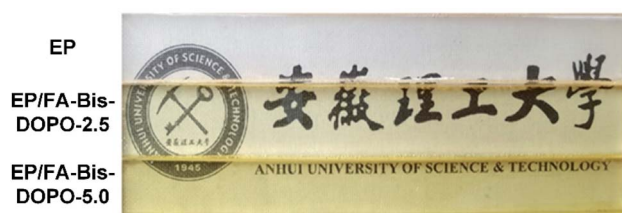


Fig. 5 Photographs of the cured epoxy thermosets.

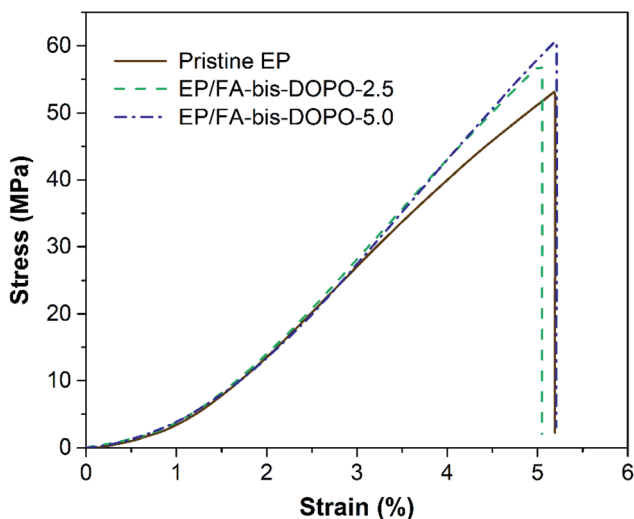
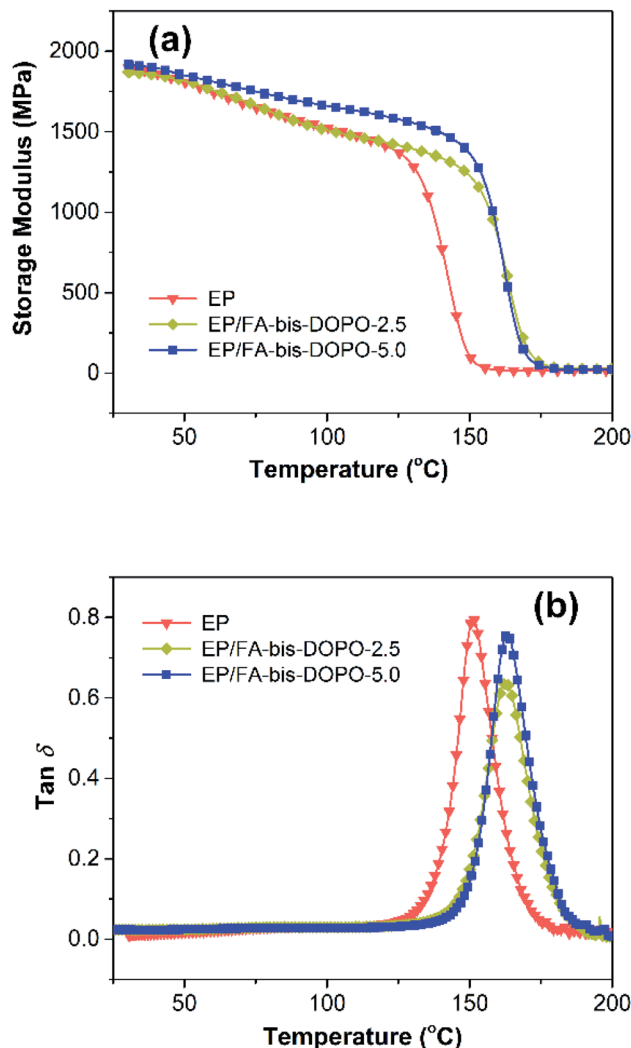


Fig. 6 The typical stress–strain curves of the pristine epoxy, EP/FA-bis-DOPO-2.5, and EP/FA-bis-DOPO-5.0.

pristine epoxy thermoset shows a fracture strength of  $53.04 \pm 2.16$  MPa. The addition of FA-bis-DOPO slightly increases the fracture strength to  $57.20 \pm 1.72$  MPa for the EP/FA-bis-DOPO-2.5 and  $60.76 \pm 2.04$  MPa for the EP/FA-bis-DOPO-5.0. The increased fracture strength proves the excellent compatibility of FA-bis-DOPO with the epoxy matrix, because the FA-bis-DOPO takes part in the curing reaction to form an integrated crosslinking network. Besides, the rich aromatic structure of FA-bis-DOPO is another reason for the improved fracture strength. The strain at break of all the samples is in the range of 5.1–5.2%, indicating the brittle nature of these epoxy thermosets.

The effect of FA-bis-DOPO on the thermos-mechanical properties of the cured epoxy thermosets was studied by the dynamic mechanical analysis. Fig. 7 shows storage modulus and  $\tan \delta$  versus temperature plots of the cured epoxy thermosets, and Table 3 lists the thermos-mechanical data. As shown in Fig. 7a, the storage modulus at 30 °C of the pristine epoxy is 1896.2 MPa, while it is 1869.7 and 1917.2 MPa for EP/FA-bis-DOPO-2.5 and EP/FA-bis-DOPO-5.0, respectively. The rigid structure of phosphaphenanthrene and furan ring is responsible for the increased storage modulus. With increasing the temperature, all the samples exhibit a sharp decreasing trend in the storage modulus, corresponding to the transition from the glassy state to the rubbery state of the cured epoxy networks.

Fig. 7 (a) Storage modulus and (b)  $\tan \delta$  versus temperature plots of the cured epoxy thermosets.

The storage modulus at 30 °C beyond the glass transition temperature ( $T_g$ ) shows a similar trend to that at 30 °C.  $T_g$  can be determined by the temperature at the peak value of the  $\tan \delta$  plots (Fig. 7b). It is found that the addition of FA-bis-DOPO increases the  $T_g$  value of the cured epoxy thermosets. This is because the secondary amine in the FA-bis-DOPO structure could participate in the curing reaction with epoxy matrix, thus increasing the crosslinking density. To verify this conjecture, the crosslinking density ( $v_c$ ) is calculated using the following formula:<sup>36</sup>

$$v_c = E'/3RT$$

where  $R$  is the universal gas constant,  $E'$  is the storage modulus at 30 °C beyond the  $T_g$ , and  $T$  is the Kelvin temperature. It is proved that the crosslinking density of the cured epoxy thermosets gradually increases with the increment of FA-bis-DOPO.

The thermal degradation behaviors of the epoxy thermosets were investigated by TGA technique. The TGA and DTG profiles



Table 3 Thermo-mechanical parameters of the pure EP and its composites

Sample	$T_g$ (°C)	$E'$ at 30 °C (MPa)	$E'$ at $T_g + 30$ °C (MPa)	$v_c$ (mol m <sup>-3</sup> )
EP	151 ± 2	1896.2 ± 21.0	15.0 ± 0.3	1.32 × 10 <sup>3</sup>
EP/FA-bis-DOPO-2.5	163 ± 2	1869.7 ± 27.4	22.1 ± 0.4	1.90 × 10 <sup>3</sup>
EP/FA-bis-DOPO-5.0	163 ± 2	1917.2 ± 18.3	26.6 ± 0.3	2.29 × 10 <sup>3</sup>

of the epoxy thermosets under the nitrogen and air atmospheres are given in Fig. 8. All the epoxy thermosets display one single thermal degradation stage in the temperature range from 320 to 465 °C. This dominant thermal degradation stage (approximately 80 wt% weight loss) is corresponding to the breakage of macromolecular chains of the epoxy networks into several small molecular volatiles including allyl alcohol, acetone, ethers, methane, *etc.* It can be seen from Table 4 that the temperature of 5 wt% weight loss ( $T_{5\%}$ ) of the epoxy thermosets is reduced with increasing the FA-bis-DOPO amount. This is because the thermally labile DOPO unit is prone to decompose in advance compared to the epoxy matrix. The earlier thermal degradation of FA-bis-DOPO catalyzes the char formation, as evidenced by the increased char residues at high temperature. Additionally, it can be seen from the differential TGA curves that the presence of FA-bis-DOPO decreases the maximum weight loss rate during the thermal degradation process. All the epoxy thermosets behave a quite different thermal degradation behavior under the air from that under the nitrogen. All the epoxy thermosets exhibit a two-stage thermal degradation process under the air. The first stage in the temperature range of 320–450 °C (approximately 60 wt% weight loss), which is corresponding to the split of the cross-linked structure of epoxy networks into several small molecular volatiles under the acid-catalyzed de-polymerization reaction. The second one in the temperature range of 500–650 °C (about 38 wt% weight loss) is corresponding to the oxidative degradation of the residual chars. Additionally, the presence of FA-bis-DOPO also decreases the maximum weight loss rate during the thermal degradation process as observed from the differential TGA curves.

The flame-retardant behaviors of the LOI and UL-94 vertical burning test are summarized in Table 5. The pristine epoxy thermoset cannot self-extinct until the flame reaches the top of the sample, implying it fails in the UL-94 vertical burning test. Besides, the LOI value of the pristine epoxy thermoset is around

second ignition is 12 and 6 s, respectively, qualifying the UL-94 V-1 grade. With further increasing the FA-bis-DOPO amount to 5.0 wt%, the LOI of the resulting epoxy thermoset is also increased to 31.0%. The EP/FA-bis-DOPO-5.0 can self-extinct within 3 s after the first and second ignition, achieving the UL-94 V-0 grade. Additionally, the addition of FA-bis-DOPO can inhibit the melt dripping behavior of the epoxy composites during the combustion. These results demonstrate that FA-bis-DOPO endows the epoxy substrate with superior flame resistance.

Cone calorimeter is further employed to study the effect of FA-bis-DOPO on the flammability of the epoxy thermosets. Table 6 lists the typical parameters including time to ignition ( $t_{ig}$ ), peak value of heat release rate (PHRR), total heat release (THR), total smoke production (TSP), and mean effective heat of combustion (EHC). The heat release rate (HRR), THR, TSP and mass loss rate of the epoxy thermosets are plotted with time in Fig. 9. As shown in Fig. 9a and Table 6, the epoxy thermosets containing FA-bis-DOPO exhibit a lower  $t_{ig}$  than the pristine epoxy, which could be ascribed to the earlier thermal decomposition of FA-bis-DOPO as indicated in TGA test. The HRR curve of the pristine epoxy shows a sharp peak with the value of 968 kW m<sup>-2</sup>. After incorporating FA-bis-DOPO, the PHRR values of EP/FA-bis-DOPO-2.5 and EP/FA-bis-DOPO-5.0 are decreased to 866 and 697 kW m<sup>-2</sup>, respectively, corresponding to a 10.5% and 28.0% reduction compared to that of pure EP. The THR values of the epoxy thermosets show a similar trend to the PHRR ones. As shown in Fig. 9b, the THR of the pristine epoxy is 157.5 MJ m<sup>-2</sup>, while the THR values of EP/FA-bis-DOPO-2.5 and EP/FA-bis-DOPO-5.0 are decreased to 136.9 and 114.5 MJ m<sup>-2</sup>, respectively, corresponding to a 13.1% and 27.3% reduction compared to that of the pristine EP. The flame retardancy index (FRI) has been employed to quantitatively characterize the flame retardant efficiency of polymers on the basis of cone calorimeter data, which can be calculated according to the eqn (1):<sup>37</sup>

$$\text{Flame retardancy index (FRI)} = \frac{[\text{THR} \times (\text{PHRR}/t_{ig})]_{\text{EP}}}{[\text{THR} \times (\text{PHRR}/t_{ig})]_{\text{EP/FA-bis-DOPO}}} \quad (1)$$

23.5%. After adding 2.5 wt% FA-bis-DOPO, the LOI value of the resulting epoxy thermoset grows sharply to 29.0%, and the sample can self-extinguish in the UL-94 vertical burning test. The burning time of the EP/FA-bis-DOPO-2.5 after the first and

The FRI of EP/FA-bis-DOPO-2.5 and EP/FA-bis-DOPO-5.0 is determined to be 1.26 and 1.31, respectively, corresponding to the “Good” flame retardancy ( $1 < \text{FRI} < 10$ ) [ ].



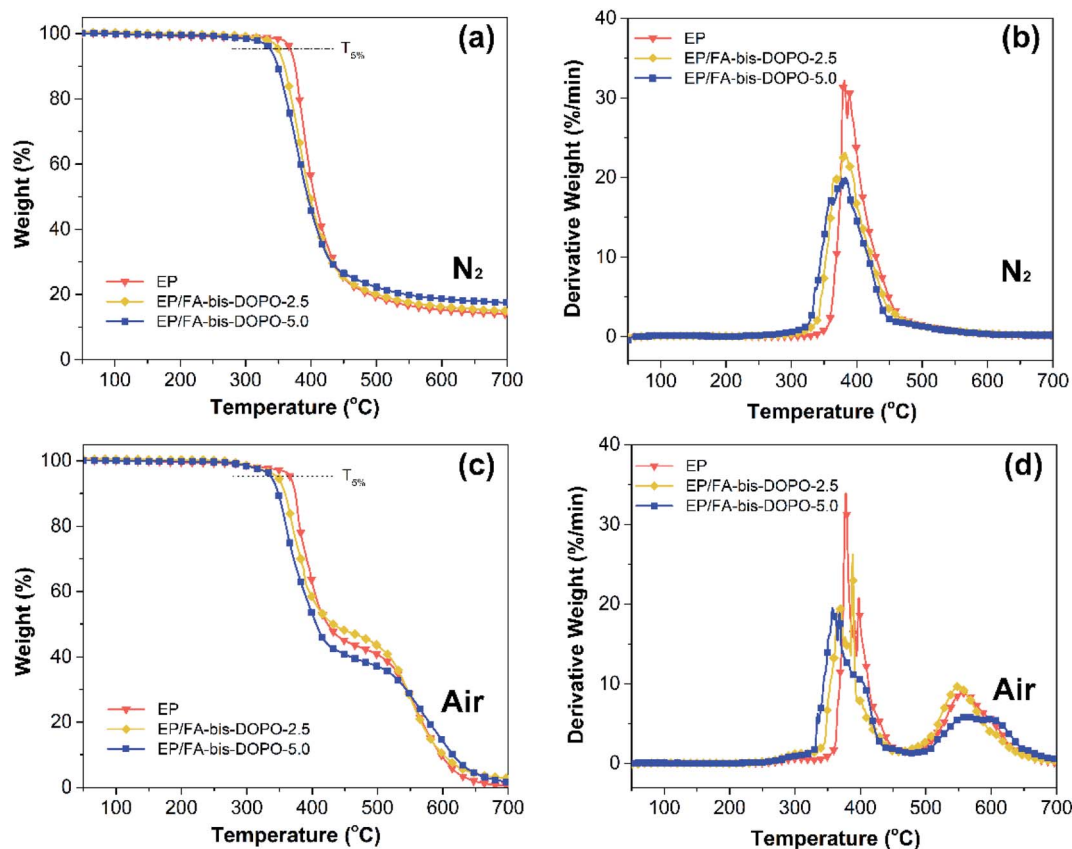


Fig. 8 (a, c) TGA and (b, d) DTG profiles of the epoxy thermosets under the nitrogen and air atmospheres.

Besides the suppressed heat release rate, the addition of FA-bis-DOPO also decreases the smoke emission of epoxy matrix. As shown in Fig. 9c, the TSP of the pristine EP is 33.2 m<sup>2</sup>, while the TSP values of EP/FA-bis-DOPO-2.5 and EP/FA-bis-DOPO-5.0 are 30.6 and 29.9 m<sup>2</sup>, respectively, which are 7.8% and 9.9% lower than that of the pristine EP. As shown in Fig. 9d, the char yield of the pristine EP is about 5.2%, whereas that of EP/FA-bis-DOPO-5.0 is increased to 9.1%. The increased char yield not only implies that less epoxy matrix is converted into pyrolysis gas to provide fuel and smoke sources, but also plays a barrier role in suppressing heat and smoke release. Mean EHC is an indicator of flame suppression in the vapor phase.<sup>38,39</sup> As shown in Table 6, the mean EHC values of EP/FA-bis-DOPO-2.5 and EP/

FA-bis-DOPO-5.0 are lower than that of the pristine EP, implying that FA-bis-DOPO also acts in the vapor phase. This is because the DOPO unit could emit PO<sup>•</sup> radicals to quench the H<sup>•</sup> and OH<sup>•</sup> radicals.<sup>40</sup> Thus, it can be concluded that the good flame retardant efficacy of FA-bis-DOPO is attributed to the combined condensed- and vapor-phase mechanisms.

TGA-FTIR was utilized to identify the pyrolytic volatile products of the pristine EP and EP/FA-bis-DOPO-5.0 during the thermal decomposition process. The three-dimensional FTIR spectra of the pyrolytic volatile products of the pristine EP and EP/FA-bis-DOPO-5.0 are shown in Fig. 10a and b. Some strong characteristic bands are observed at the wavenumber range of 3700–3400, 3100–2800, 1800–1700, 1650–1450, and 1300–

Table 4 TGA and DTG data of the epoxy samples under the nitrogen and air atmospheres

Samples	$T_{5\%}$ (°C)		$T_{max}$ (°C)		Residues (%) at 700 °C	
	N <sub>2</sub>	Air	N <sub>2</sub>	Air	N <sub>2</sub>	Air
EP	369	367	381	378, 558	14.0	0.6
EP/FA-bis-DOPO-2.5	350	348	381	389, 550	14.9	2.6
EP/FA-bis-DOPO-5.0	338	338	380	359, 558	17.5	1.9

Table 5 The results of the LOI and UL-94 vertical burning test of the cured epoxy systems

		UL-94		
Sample	LOI (%)	$t_1 + t_2^a$	Dripping	Rating
EP	23.5	Burning to clamp	Yes	Failed
EP/FA-bis-DOPO-2.5	29.0	12 + 6	No	V-1
EP/FA-bis-DOPO-5.0	31.0	3 + 3	No	V-0

<sup>a</sup>  $t_1$  and  $t_2$  mean the burning time after the first and second ignition, respectively.



Table 6 The cone calorimeter data of the cured epoxy systems

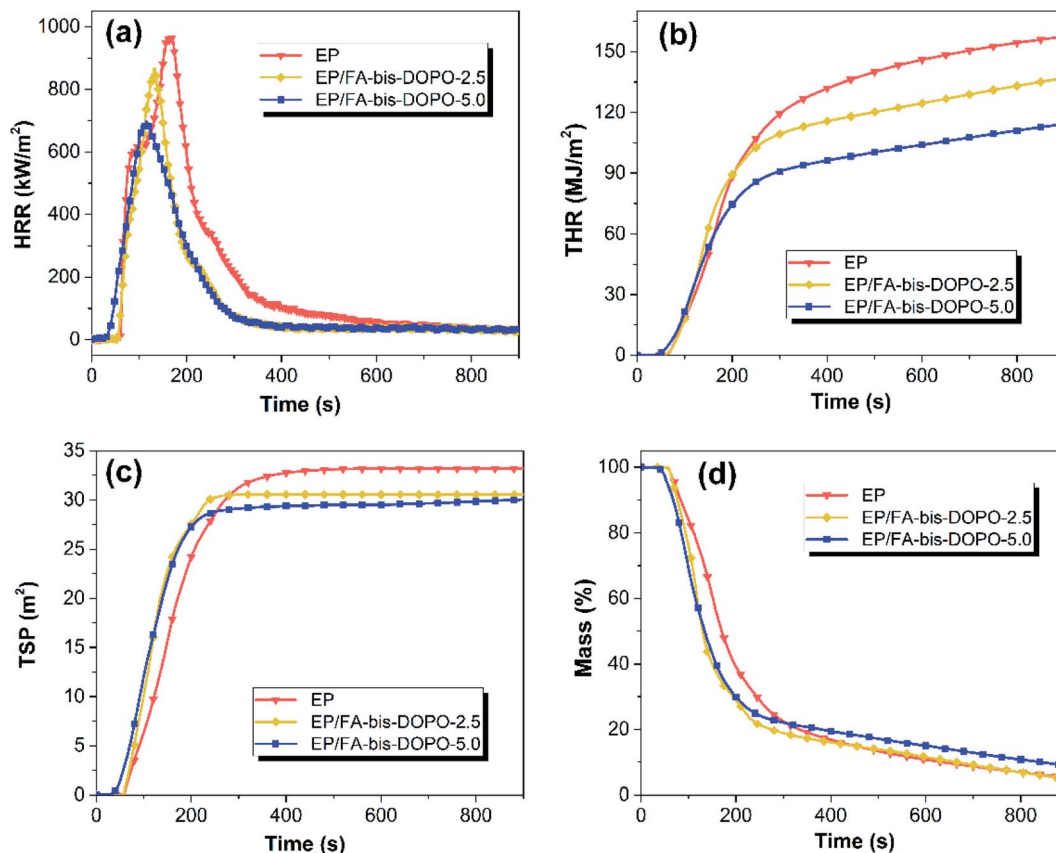
Samples	$t_{ig}$ (s)	PHRR ( $\text{kW m}^{-2}$ )	THR ( $\text{MJ m}^{-2}$ )	FRI	TSP ( $\text{m}^2$ )	Mean EHC ( $\text{MJ kg}^{-1}$ )	Residue (wt%)
EP	57	968	157.5	—	33.2	35.5	5.2
EP/FA-bis-DOPO-2.5	56	866	136.9	1.26	30.6	32.3	5.2
EP/FA-bis-DOPO-5.0	39	697	114.5	1.31	29.9	31.0	9.1

$1100\text{ cm}^{-1}$ . The FTIR spectra of the pyrolytic volatile products of the pristine EP and EP/FA-bis-DOPO-5.0 at the maximum decomposition rate are depicted in Fig. 10c. Some characteristic volatile products including water ( $3650\text{ cm}^{-1}$ ), methyl- and/or methylene-containing compounds ( $2975\text{ cm}^{-1}$ ), carbonyl-containing compounds ( $1730\text{ cm}^{-1}$ ), aromatic compounds ( $1605$  and  $1510\text{ cm}^{-1}$ ), and ethers ( $1175\text{ cm}^{-1}$ ) are emitted.<sup>2,41</sup> By comparing the shape and position of the FTIR spectrum of EP/FA-bis-DOPO-5.0 with those of the pristine EP, it can be found that the addition of FA-bis-DOPO almost does not change the types of the pyrolytic gas products.

In order to further clarify the influence of FA-bis-DOPO on the thermal decomposition products of the epoxy matrix, the absorbance intensity of several typical pyrolytic products *versus* time curves of the pristine EP and EP/FA-bis-DOPO-5.0 is provided in Fig. 11. It can be seen that the relative intensity of the typical pyrolytic volatile products including methyl- and/or

methylene-containing compounds ( $2975\text{ cm}^{-1}$ ), carbonyl-containing compounds ( $1730\text{ cm}^{-1}$ ), aromatic compounds ( $1510\text{ cm}^{-1}$ ), and ethers ( $1175\text{ cm}^{-1}$ ) is much lower as compared to that of the pristine EP. According to the Beer-Lambert law, the lower absorbance intensity means the less pyrolytic volatile products concentration. Because these typical pyrolytic volatile products are all combustible gases that are the major source of fuel, the less pyrolytic volatile products concentration implies the less fuel supply. This is why the EP/FA-bis-DOPO-5.0 composite behaves much lower PHRR and THR than the pristine EP.

The morphological feature of the residual chars formed during the combustion plays a crucial role in the flame retardant performance. Fig. 12 depicts the SEM micrographs of the residual chars of (a) pristine epoxy, (b) EP/FA-bis-DOPO-2.5, and (c) EP/FA-bis-DOPO-5.0. As can be observed, the surface of the residual char of the pristine epoxy thermoset is full of holes,

Fig. 9 (a) HRR, (b) THR, (c) TSP, and (d) mass loss *versus* time curves of the cured epoxy thermosets.



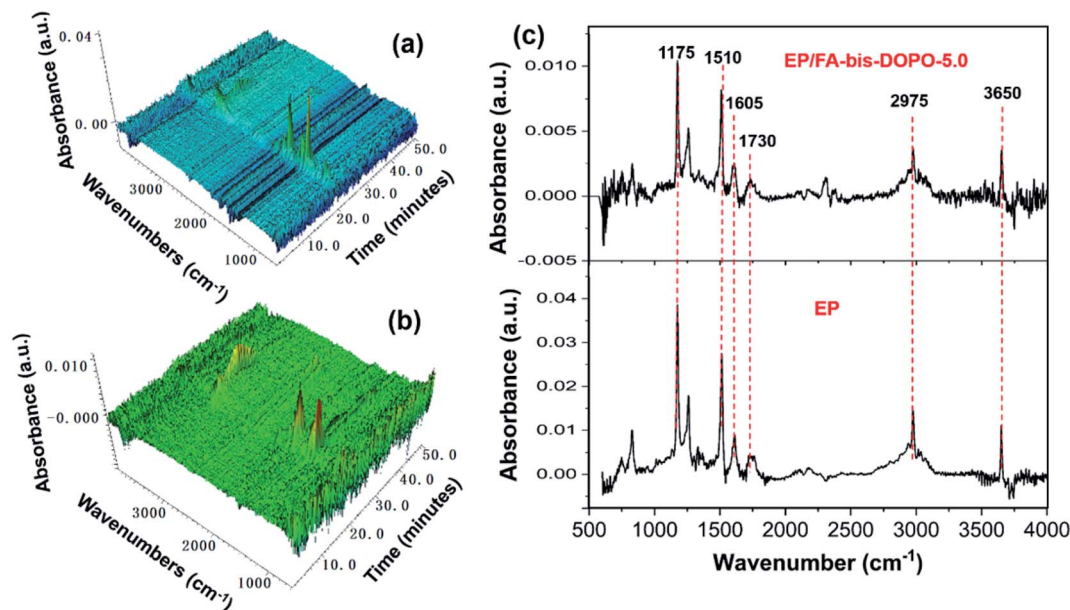


Fig. 10 Three-dimensional FTIR spectra of the pyrolytic volatile products of (a) pristine EP and (b) EP/FA-bis-DOPO-5.0; (c) FTIR spectra of the pyrolytic volatile products of pristine EP and EP/FA-bis-DOPO-5.0 at the maximum decomposition rate.

which could be caused by the pyrolytic gases volatilization from the violent thermal degradation of the epoxy substrate. The pyrolytic gases diffuse from these holes to supply the combustion as fuel. That is why the pristine epoxy thermoset shows so high PHRR and THR values. The residual char of the EP/FA-bis-DOPO-2.5 is still fragmented, with some cracks and holes distributed on the surface. Such the morphological feature still

cannot stop the diffusion of pyrolytic gases escape to feed the combustion. By contrast, the residual char of the EP/FA-bis-DOPO-5.0 is intact and compact without visible holes, which is conducive to the suppression of the release of the pyrolytic gases. Consequently, the EP/FA-bis-DOPO-5.0 behaves the lowest PHRR and THR values during the combustion.

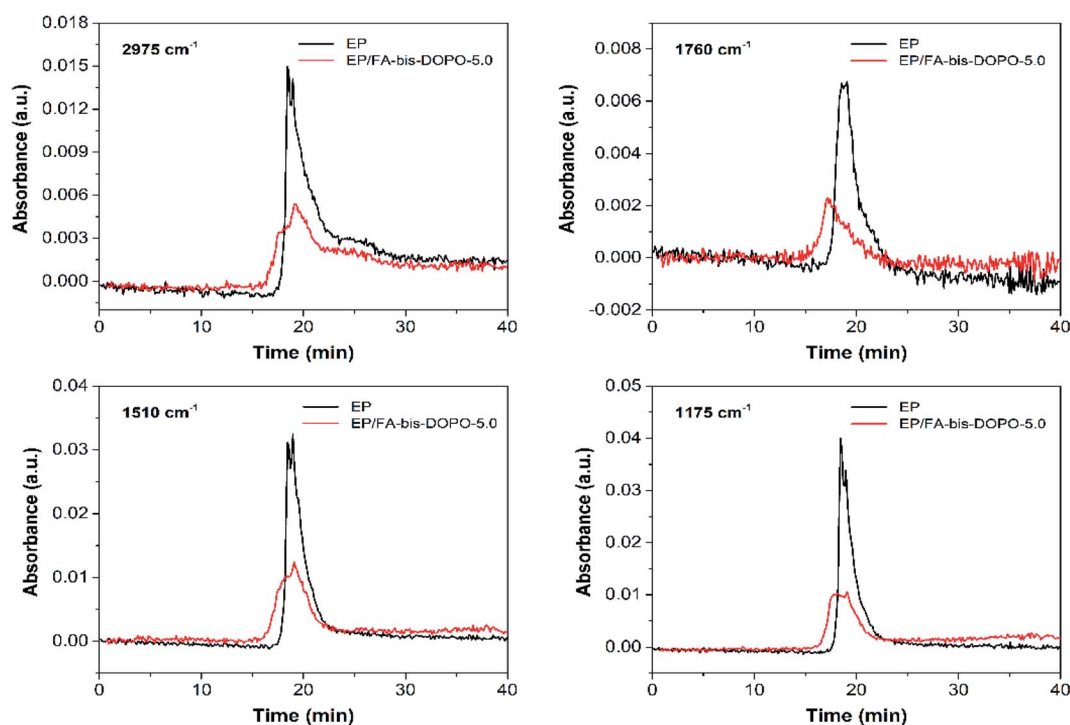


Fig. 11 Absorbance intensity of several typical pyrolytic products versus time curves of the pristine EP and EP/FA-bis-DOPO-5.0.

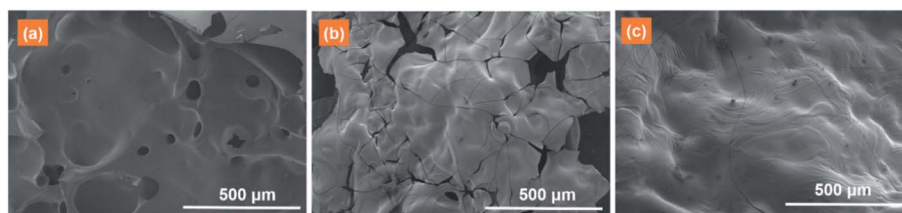


Fig. 12 SEM micrographs of the residual chars of (a) pristine epoxy, (b) EP/FA-bis-DOPO-2.5, and (c) EP/FA-bis-DOPO-5.0.

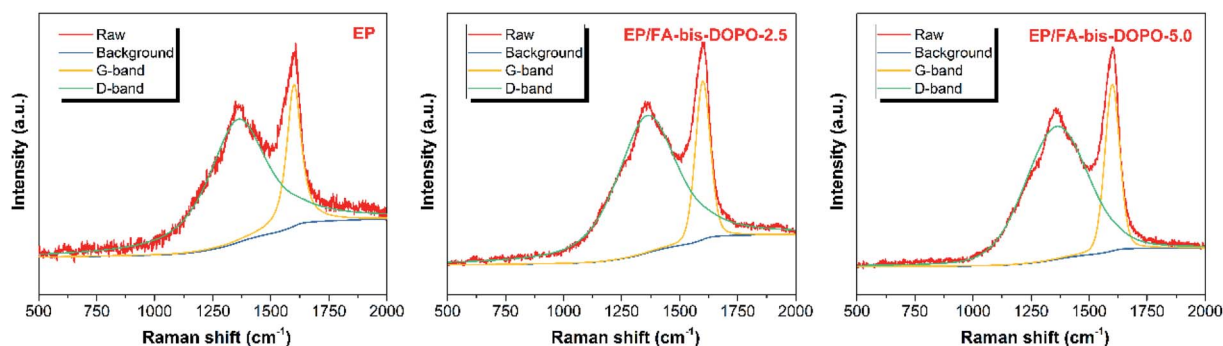


Fig. 13 Raman spectra of the residual chars of pristine epoxy, EP/FA-bis-DOPO-2.5, and EP/FA-bis-DOPO-5.0.

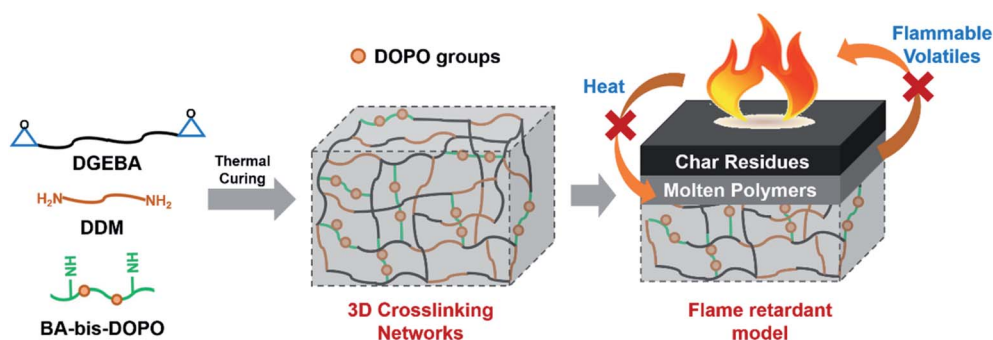


Fig. 14 Diagrammatical representation of the flame retardant mechanism of EP/FA-bis-DOPO.

Raman spectrometer was further employed to characterize the microstructure of the residual chars to clarify the flame retardant mechanism. Fig. 13 shows the Raman spectra of the residual chars of pristine epoxy, EP/FA-bis-DOPO-2.5, and EP/FA-bis-DOPO-5.0. All the samples exhibit two dominant bands at around 1360 and 1600  $\text{cm}^{-1}$  in their Raman spectra. The former is called D-band that corresponds to the amorphous structure consisted of the disordered carbon atoms, while the latter is called G-band that is related to the scattering of the crystalline structure consisted of the graphitized carbon atoms.<sup>42</sup> The graphitization degree of the residual chars could be assessed using the intensity ratio between the D-band and G-band ( $I_D/I_G$ ).<sup>43–45</sup> The  $I_D/I_G$  value of the residual chars obeys the sequence of pristine epoxy (4.25) > EP/FA-bis-DOPO-2.5 (4.13) > EP/FA-bis-DOPO-5.0 (3.39). The higher  $I_D/I_G$  value represents the lower graphitization degree. So, the residual char of the EP/FA-bis-DOPO-5.0 contains more graphitized structure,

which is conducive to the better thermal resistance of the char. The char with higher thermal resistance could serve as a better insulating layer to shield the underlying materials from thermal decomposition, thus alleviating the intensity of combustion.

On the basis of the above discussion, a possible flame retardant mechanism of EP/FA-bis-DOPO was proposed, as represented in Fig. 14. According to the calculated CI values, FA-bis-DOPO could participated in the curing reaction with DGEBA and DDM to form an excellent or good 3D crosslinking networks. When heated, the 3D crosslinking networks broke to emit the phosphorus-containing species that acted as a char promoter. Thus, an intact and dense char layer was formed covering on the surface of the molten polymers as a barrier for flammable volatiles and heat exchange. As a result of the presence of the char layer, the flame retardant behavior of EP/FA-bis-DOPO was notably enhanced.



## 4. Conclusions

In this study, a novel furfurylamine-derived bis-DOPO derivative (FA-bis-DOPO) was synthesized successfully and applied as a curing agent for flame retardant epoxy resins. Owing to the rigidity and the reactivity of FA-bis-DOPO, the addition of FA-bis-DOPO could enhance the mechanical strength, the storage modulus and the glass transition temperature of the flame retardant epoxy materials. With 5.0 wt% incorporation of FA-bis-DOPO, the epoxy thermoset achieved an LOI of 31.0% and a UL-94 V-0 rating, whereas the pristine EP had a much lower LOI of 23.5% and no rating in the UL-94 test. In the cone calorimeter test, the PHRR, THR, and TSP values of the EP/FA-bis-DOPO-5.0 were declined by 28.0%, 27.3%, and 9.9%, respectively, as compared to those of the pristine EP. The good flame retardant efficiency of FA-bis-DOPO could be ascribed to the combined vapor and condensed flame retardant mechanisms: DOPO unit could emit PO<sup>•</sup> radicals to quench the combustion chain reactions in the vapor phase, and it could also catalyze epoxy substrate to form an intact and compact char layer in the condensed phase that served as a protective barrier to inhibit the transfer of pyrolytic volatile products. This furfurylamine-derived bis-DOPO derivative provides a promising solution for highly efficient flame retardant epoxy thermosets with excellent comprehensive performances.

## Conflicts of interest

No conflict of interest exists in this manuscript.

## Acknowledgements

The authors gratefully acknowledge the National Natural Science Foundation of China (52074011), Anhui Provincial Natural Science Foundation (1908085J20), University Synergy Innovation Program of Anhui Province (GXXT-2020-057, GXXT-2020-079).

## References

- 1 X. Wang, Y. Hu, L. Song, W. Xing, H. Lu, P. Lv and G. Jie, *Polymer*, 2010, **51**, 2435–2445.
- 2 X. Wang, Y. Hu, L. Song, W. Xing and H. Lu, *J. Anal. Appl. Pyrolysis*, 2011, **92**, 164–170.
- 3 X. Wang, Y. Hu, L. Song, H. Yang, W. Xing and H. Lu, *Prog. Org. Coat.*, 2011, **71**, 72–82.
- 4 S. Nie, D. Jin, Y. Xu, C. Han, X. Dong and J.-n. Yang, *J. Mater. Res. Technol.*, 2020, **9**, 10189–10197.
- 5 S. M. Seraji, H. Gan, S. R. Swan and R. J. Varley, *React. Funct. Polym.*, 2021, **164**, 104910.
- 6 E. R. Rad, H. Vahabi, A. R. de Anda, M. R. Saeb and S. Thomas, *Prog. Org. Coat.*, 2019, **135**, 608–612.
- 7 H. Vahabi, M. Jouyandeh, M. Cochez, R. Khalili, C. Vagner, M. Ferriol, E. Movahedifar, B. Ramezanzadeh, M. Rostami, Z. Ranjbar, B. S. Hadavand and M. R. Saeb, *Prog. Org. Coat.*, 2018, **123**, 160–167.
- 8 H. Vahabi, M. R. Saeb, K. Formela and J.-M. L. Cuesta, *Prog. Org. Coat.*, 2018, **119**, 8–14.
- 9 L. Gu, G. Chen and Y. Yao, *Polym. Degrad. Stab.*, 2014, **108**, 68–75.
- 10 X. Li, Y. Ou and Y. Shi, *Polym. Degrad. Stab.*, 2002, **77**, 383–390.
- 11 S. V. Levchik and E. D. Weil, *J. Fire Sci.*, 2006, **24**, 345–364.
- 12 M. M. Velencoso, A. Battig, J. C. Markwart, B. Scharrel and F. R. Wurm, *Angew. Chem., Int. Ed.*, 2018, **57**, 10450–10467.
- 13 S. M. Seraji, H. Gan, S. Issazadeh and R. J. Varley, *Macromol. Chem. Phys.*, 2021, **222**, 2000342.
- 14 K. A. Salmeia and S. Gaan, *Polym. Degrad. Stab.*, 2015, **113**, 119–134.
- 15 S. Yang, J. Wang, S. Q. Huo, M. Wang and L. F. Cheng, *Ind. Eng. Chem. Res.*, 2015, **54**, 7777–7786.
- 16 M. J. Xu, G. R. Xu, Y. Leng and B. Li, *Polym. Degrad. Stab.*, 2016, **123**, 105–114.
- 17 L. J. Qian, Y. Qiu, N. Sun, M. L. Xu, G. Z. Xu, F. Xin and Y. J. Chen, *Polym. Degrad. Stab.*, 2014, **107**, 98–105.
- 18 S. P. Teong, G. S. Yi and Y. G. Zhang, *Green Chem.*, 2014, **16**, 2015–2026.
- 19 P. Wang and Z. Cai, *Polym. Degrad. Stab.*, 2017, **137**, 138–150.
- 20 J. J. Zhang, H. J. Duan, J. F. Cao, J. H. Zou and H. R. Ma, *J. Appl. Polym. Sci.*, 2021, **138**, 50165.
- 21 H. Tang, Z. Zhu, R. Chen, J. Wang and H. Zhou, *Polym. Adv. Technol.*, 2019, **30**, 2331–2339.
- 22 M. Jouyandeh, M. Shabanian, M. Khaleghi, S. M. R. Paran, S. Ghiyasi, H. Vahabi, K. Formela, D. Puglia and M. R. Saeb, *Prog. Org. Coat.*, 2018, **125**, 384–392.
- 23 M. Jouyandeh, S. M. R. Paran, A. Jannesari, D. Puglia and M. R. Saeb, *Prog. Org. Coat.*, 2019, **131**, 333–339.
- 24 F. Seidi, M. Jouyandeh, M. Taghizadeh, A. Taghizadeh, H. Vahabi, S. Habibzadeh, K. Formela and M. R. Saeb, *Materials*, 2020, **13**, 2881.
- 25 S. Farzad, J. Maryam, T. Ali, T. Mohsen, H. Sajjad, J. Yongcan, X. Huining, Z. Payam and S. M. Reza, *Surf. Innovations*, 2021, **9**, 3–16.
- 26 R. Wazalwar, N. Tripathi and A. M. Raichur, *Composites Part C: Open Access*, 2021, **5**, 100128.
- 27 M. Ganjaee Sari, H. Vahabi, X. Gabrion, P. Laheurte, P. Zarrintaj, K. Formela and M. R. Saeb, *Prog. Org. Coat.*, 2018, **119**, 171–182.
- 28 H. Rastin, M. R. Saeb, M. Nonahal, M. Shabanian, H. Vahabi, K. Formela, X. Gabrion, F. Seidi, P. Zarrintaj, M. G. Sari and P. Laheurte, *Prog. Org. Coat.*, 2017, **113**, 126–135.
- 29 M. Nonahal, H. Rastin, M. R. Saeb, M. G. Sari, M. H. Moghadam, P. Zarrintaj and B. Ramezanzadeh, *Prog. Org. Coat.*, 2018, **114**, 233–243.
- 30 F. Tikhani, M. Jouyandeh, S. H. Jafari, S. Chabokrow, M. Ghahari, K. Gharanjig, F. Klein, N. Hampp, M. R. Ganjali, K. Formela and M. R. Saeb, *Prog. Org. Coat.*, 2019, **135**, 176–184.
- 31 Z. Karami, M. Jouyandeh, J. A. Ali, M. R. Ganjali, M. Aghazadeh, M. Maadani, M. Rallini, F. Luzi, L. Torre, D. Puglia, V. Akbari and M. R. Saeb, *Prog. Org. Coat.*, 2019, **136**, 105228.



- 32 M. Jouyandeh, F. Tikhani, N. Hampp, D. Akbarzadeh Yazdi, P. Zarrintaj, M. Reza Ganjali and M. Reza Saeb, *Chem. Eng. J.*, 2020, **396**, 125196.
- 33 M. Jouyandeh, O. M. Jazani, A. H. Navarchian, M. Shabanian, H. Vahabi and M. R. Saeb, *Appl. Surf. Sci.*, 2019, **479**, 1148–1160.
- 34 A. A. Abdi, M. Jouyandeh, H. Vahabi, M. Shabanian, D. Lafon-Pham, X. Gabrion, P. Laheurte, A. M. Nahavandi and M. R. Saeb, *J. Inorg. Organomet. Polym. Mater.*, 2021, **31**, 923–933.
- 35 M. Jouyandeh, N. Rahmati, E. Movahedifar, B. S. Hadavand, Z. Karami, M. Ghaffari, P. Taheri, E. Bakhshandeh, H. Vahabi, M. R. Ganjali, K. Formela and M. R. Saeb, *Prog. Org. Coat.*, 2019, **133**, 220–228.
- 36 S. Ma, X. Liu, Y. Jiang, L. Fan, J. Feng and J. Zhu, *Sci. China: Chem.*, 2014, **57**, 379–388.
- 37 E. Movahedifar, H. Vahabi, M. R. Saeb and S. Thomas, *Molecules*, 2019, **24**, 3964.
- 38 L. Zhong, K.-X. Zhang, X. Wang, M.-J. Chen, F. Xin and Z.-G. Liu, *J. Therm. Anal. Calorim.*, 2018, **134**, 1637–1646.
- 39 W. Xu, R. Chen, Y. Du and G. Wang, *Polym. Degrad. Stab.*, 2020, **176**, 109152.
- 40 S. Liu, B. Yu, Y. Feng, Z. Yang and B. Yin, *Polym. Degrad. Stab.*, 2019, **165**, 92–100.
- 41 Z. Zhang, C. J. Wang, G. Huang, H. R. Liu, S. L. Yang and A. F. Zhang, *J. Hazard. Mater.*, 2018, **357**, 73–80.
- 42 X. Wang, S. Zhou, W. Xing, B. Yu, X. Feng, L. Song and Y. Hu, *J. Mater. Chem. A*, 2013, **1**, 4383–4390.
- 43 Z. Xu, W. Xing, Y. Hou, B. Zou, L. Han, W. Hu and Y. Hu, *Combust. Flame*, 2021, **226**, 108–116.
- 44 G. Tang, X. Liu, L. Zhou, P. Zhang, D. Deng and H. Jiang, *Adv. Powder Technol.*, 2020, **31**, 279–286.
- 45 G. Tang, X. Liu, Y. Yang, D. Chen, H. Zhang, L. Zhou, P. Zhang, H. Jiang and D. Deng, *Adv. Powder Technol.*, 2020, **31**, 1420–1430.

